Biomedical Physics & Engineering Express

Endorsed by IPEM Institute of Physics and Engineering in Medicine

PAPER • **OPEN ACCESS**

Self-made transparent optoacoustic detector for measurement of skin lesion thickness *in vivo*

To cite this article: Anatoly Fedorov Kukk *et al* 2022 *Biomed. Phys. Eng. Express* **8** 035029

View the article online for updates and enhancements.

You may also like

- Efficient non-negative constrained model-based inversion in optoacoustic tomography
Lu Ding, X Luís Deán-Ben, Christian Lutzweiler et al.
- Listening to tissues with new light: recent technological advances in photoacoustic imaging
Tri Vu, Daniel Razansky and Junjie Yao
- Estimation of optoacoustic contrast agent concentration with self-calibration blind logarithmic unmixing
X Luís Deán-Ben, Andreas Buehler, Daniel Razansky et al.

2023 Radformation Developer Summit
In-person before the AAPM Annual Meeting
RADformation
Dr. Kundan Thind
Dr. Matthew C Schmidt
Dr. Sarah Quirk
Wayne Keranen
Presentations, panel discussion, breakout sessions, happy hour, and more!
All Experience Levels Welcome
Register Now →

This content was downloaded from IP address 194.95.157.34 on 31/07/2023 at 07:34

Biomedical Physics & Engineering Express

PAPER

Self-made transparent optoacoustic detector for measurement of skin lesion thickness *in vivo*

Anatoly Fedorov Kukk[1], **Elias Blumenröther**[1] **and Bernhard Roth**[1,2]

[1] Hannover Centre for Optical Technologies, Leibniz University Hannover, Nienburger Str. 17, 30167 Hannover, Germany
[2] Cluster of Excellence PhoenixD (Photonics, Optics and Engineering - Innovation Across Disciplines), Welfengarten 1a, 30167 Hannover, Germany

E-mail: anatoly.kukk@hot.uni-hannover.de

Keywords: photoacoustics, optoacoustics, transparent detector, skin cancer depth measurements *in vivo*

OPEN ACCESS

RECEIVED
17 November 2021

REVISED
5 February 2022

ACCEPTED FOR PUBLICATION
12 April 2022

PUBLISHED
27 April 2022

Original content from this work may be used under the terms of the Creative Commons Attribution 4.0 licence.

Any further distribution of this work must maintain attribution to the author(s) and the title of the work, journal citation and DOI.

Abstract

In skin cancer diagnosis and treatment, one of the key factors is tumor depth, which is connected to the severity and the required excision depth. Optoacoustical (OA) imaging is a relatively popular technique that provides information based on the optical absorption of the sample. Although often demonstrated with *ex vivo* measurements or *in vivo* imaging on parts of small animals, *in vivo* measurements on humans are more challenging. This is presumably because it is too time consuming and the required excitation pulse energies and their number exceed the allowed maximum permissible exposure (MPE). Here, we demonstrate thickness measurements with a transparent optoacoustical detector of different suspicious skin lesions *in vivo* on patients. We develop the signal processing technique to automatically convert the raw signal into thickness via deconvolution with the impulse response function. The transparency of the detector allows optical excitation with the pulsed laser to be performed perpendicularly on the lesion, in contrast to the conventional illumination from the side. For validation, the measured results were compared to the histological thickness determined after excision. We show that this simple transparent detector allows to determine the thickness of a lesion and thus, aid the dermatologist to estimate the excision depth in the future.

1. Introduction

Skin cancer has been showing rising incidence rates, which are likely caused by the major changes in leisure time behavior since the 20th century, for instance due to vacations in areas with higher sun exposure and increased exposure to UV radiation. It is particularly dangerous as it can resemble normal nevi (birthmarks or moles) and show little to no symptoms in early phases. Melanoma skin cancer is the most dangerous type of skin cancer, which also has the highest mortality rate. Once identified, it must be surgically removed. It is critical to detect and treat melanoma as early as possible, as their progression usually leads to metastases in lymph nodes, thus drastically reducing the chances of full recovery from over 95% if discovered early, to as little as 10% in the last stages [1, 2].

One of the most important factors, which already plays a role in primary excision, is the depth of invasion of the cancer. This cannot be measured precisely by non-invasive dermoscopic examination at the surface, and is only estimated with the Clark scale and Breslow thickness metrics [3]. Currently, the only reliable method for diagnosis is the excision of a sample of the suspicious lesion and its histological examination, which is considered as the gold standard for diagnosis. This procedure is not only invasive and painful for the patient, but also time-consuming, as several appointments and excisions are required, in case of a positive cancer result. This also represents a delay of the treatment and can have an effect on the healing chances. If the dermatologist had the prior knowledge of the cancer penetration depth, all of the affected tissue could be removed during the first excision. In various studies several non-invasive techniques for evaluation of lesion depth were tested. For example, Meyer *et al* have demonstrated good level of agreement of high-frequency ultrasound (HFUS) measurements with histological results, while optical coherence tomography (OCT) was shown to be inappropriate for lesion thicknesses over 0.5 mm [4]. Bozsányi *et al* have

© 2022 The Author(s). Published by IOP Publishing Ltd

successfully applied multispectral imaging for measuring and classifying the Breslow thickness of melanoma ($\leqslant$1 mm, 1–2 mm and $>$2 mm) [5]. Finally, multiphoton and confocal microscopy were employed for imaging of melanoma; they were however restricted to relatively low penetration depths of 200 μm in pigmented skin [6–8].

One of the possible techniques for measurement of skin cancer depth is optoacoustics (OA), which is also referred to as photoacoustics (PA). It is caused by the partial conversion of photon energy into mechanical shock waves. Although this effect was discovered already in 1880 by Alexander Graham Bell [9], it only started to gain relevance and interest after the discovery of lasers in 1960. With the possibility of high energy pulses in the nanosecond range, the topic of OA expanded and became a whole field, closely connected to the imaging. Numerous publications in the last decades demonstrate the high interest of researchers in the field of biomedical imaging with OA, especially regarding the optoacoustical microscopy [10–15]. In comparison with the conventional ultrasound (US) imaging, where the signal relates to the acoustical reflectivity of sample, in OA imaging, the contrast is provided by the optical absorption. For example, due to the high contrast of hemoglobin saturation it is attractive for imaging of vascular structures [16, 17].

In general, one can distinguish between two OA modalities: optoacoustical microscopy (OAM/PAM) and optoacoustical tomography (OAT/PAT). The OAM refers to creating images *en face* at a fixed depth from the detector, which is done by focusing both the excitation laser and the acoustical receiver to a shared spot inside the sample, followed by lateral scanning. This technique allows imaging at depths of several millimeters and have excellent spatial resolutions of up to several micrometers [16, 18]. The OAT is done either by adding the axial scanning to OAM or by time-resolving the obtained signals from a multi-element transducer array [19, 20]. The reported works demonstrate OAT in animal tissue at depths of as large as 12 cm [21]. The excitation pulses are delivered either coaxially using an acoustic-optical combiner/coupler [13, 22–24] or by illuminating from the side under an angle [25, 26].

However, a single-element unfocused transparent transducers for time resolved depth measurements rarely appeared in literature so far. The first proof of concept was reported by Niederhauser *et al* with a setup capable of measuring the depth profile based on the contrast of optical absorption in a layered dye phantom [27].

Most works reported so far relate to biomedical imaging demonstrating OAM/PAM of either phantoms, *ex vivo* tissues or parts of small animals under anesthesia, often specializing on blood vessel imaging. One possible reason why it is rarely demonstrated on humans or awake animals is the long measurement time and the total pulse energy: the OAM requires at least one laser pulse per pixel (or voxel if 3D imaging is performed) and usually long measurement times, ranging between 10-20 minutes [28]. For skin exposure with lasers in the visible range and pulse durations of several nanoseconds, the BAUA regulations in Germany [29] restrict the Maximum Permissible Exposure (MPE) to 20 mJ cm^{-2}. However for a train of N pulses, the exposition from each pulse must be reduced further by factor of $N^{-0.25}$, thus possibly limiting the usage of OAM *in vivo* on humans[3]. This shows the advantage of time-resolved OAT, as it yields 1D depth information (or 2D slice for a line transducers) with less pulses.

In this work, as a part of multimodal optical imaging of skin cancer, we developed and applied an unfocused transparent OA detector on human skin lesions *in vivo* that were scheduled for excision due to being suspected of developing into skin cancer. This transparent detector approach offers several advantages such as a wideband acoustic response, relatively low acoustic impedance as well as mechanical flexibility as compared to standard ultrasound transducers [31, 32]. By using signal deconvolution, it is possible to reconstruct the time resolved stress profile in the acoustical near-field as numerical simulations have shown before [33, 34]. Compared to common OATs, where large numbers of laser pulses are required, our strategy required only a single excitation shot. The transparency of the detector allows its integration with other optical modalities, for instance optical coherence tomography or Raman spectroscopy. In addition, it enables optical excitation perpendicular to the lesion, whereas the structure of normal OA detectors require excitation from the side or under an angle, adding complexity to the model [35]. In this study, the OA measurements were taken at a third of the MPE levels to accommodate with different optical modalities tested in the same setup. This approach might be valuable for future non-invasive melanoma skin cancer diagnostics and might even allow for scanning of a lesion provided that suitable beam steering is implemented.

2. Materials and methods

For the proof of concept we used a single-point transparent detector system, which has been described in detail previously [36]. In principle, the detector consists of a 10 μm thick polyvinylidene fluoride (PVDF) film, that acts as the piezoelectric element with an active area of 1 mm^2. It is sputtered with 50 nm thick indium tin oxide films that serve as electrodes on

[3] The ANSI Z136.1 standard [30] in USA states the same MPE for a single pulse; however Rule 3 (multiple-pulse scaling by $N^{-0.25}$) does not apply to skin exposure in this standard. Nevertheless, Rule 2 that limits the MPE with repeated exposures still applies, especially limiting the pulse energies of lasers with high duty cycle.

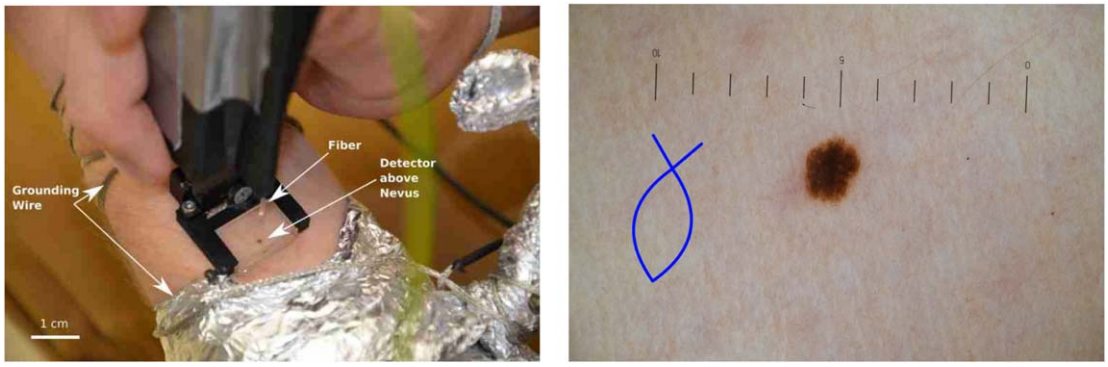

Figure 1. Left: photograph of the handheld clinical setup. On both sides of the OA setup the patient grounding is visible. Due to its high transparency, the active area of the detector film cannot be seen above the nevus. Right: image of the nevus investigated. The blue symbol is the drawing of the surgeon, indicating the orientation of the following excision and thus histology. The processed OA measurements as well as the histological result of this nevus are depicted below in figure 4.

both sides. The detector was placed into a transparent rectangular PMMA backing layer. The angular and lateral dependency were measured by shifting the detector away from the symmetry axis of the excitation beam. The results show that the OA signal drops to half of its amplitude ± 1 mm away from the center. Therefore, the detector can be treated as integrator of the OA signal from an area $<4\,\mathrm{mm}^2$ while the contribution from further lateral zones can be considered negligible. The detector was tested for depths between 0.1 mm and 6 mm with axial resolution of 50 μm [32, 37]. The optical transmission at 532 nm wavelength was measured at roughly 70%. The piezoelectrical signal was amplified with a custom amplifier and measured with a DAQ system (Agilent U1065A) at a sampling rate of 2 GHz. A pulsed single wavelength laser at 532 nm and <10 nm pulse duration (Ultra50, Quantel Laser, France) was utilized for OA excitation. The measurement and laser pulse were synchronised with a trigger signal. The laser excitation was delivered via a 880 μm thick single core fiber with numerical aperture NA $= 0.22$, with its end 18 mm above the active area of the detector. The handheld case that holds the detector block, preamplifier and the fiber holder is printed with a 3D printer with black ABS. The illuminated area was measured at 27 mm^2, which combined with the MPE level for a single pulse of 20 $\mathrm{mJ\,cm}^{-2}$ results in maximum 5.4 mJ and 3 mJ per pulse for a train of 10 pulses, respectively. Since during the *ex vivo* experiments of excised skin lesions we observed that a significant drop in signal quality occurs for energies below 0.9 mJ per pulse, we performed the *in vivo* OA measurements at 1 mJ per pulse, which is a third of the corresponding MPE level. To ensure that the maximum energy was not exceeded, it was measured simultaneously with a photodiode (S1336-18BQ, Hamamatsu Photonics) placed next to a spot on the delivery fiber. By operating the photodiode with 5 V in reverse bias, the obtained signal is well correlated to the output at the end of the fiber and therefore, allows to continuously monitor the energy output during the clinical measurement [32].

A photograph of the developed detector applied on skin is shown in figure 1. During the measurements the skin around the lesion was grounded with aluminium foil in order to reduce the background noise caused by the laser operation.

For the speed of sound in epidermal tissue, the value of $c = 1645\ \mathrm{m\,s}^{-1}$ was chosen from measurements of Moran *et al* [38]. The measured signal is processed in Python with the following steps:

1. Removal of the pyroelectric effect: since the active area of the detector is the first on the illumination path, it shows a strong but simple pyroelectric effect roughly $\tau = 1.1$ μs after the pulse start. This effect can be removed by identifying the time window of the effect and fitting it with a polynomial of 10th degree, excluding the time span of the main OA signal, as shown in figure 2 (left).

2. Deconvolution: the signal was deconvolved with the impulse response function (IRF). The IRF was previously measured as an OA signal from a black plastic block. Since the deconvolution corresponds to a division of the OA signal with the IRF in Fourier domain, the high frequency components of the IRF with extremely low magnitude result in huge amplification of noise in that spectral region, causing significant signal-to-noise degradation that is also known as ringing. This problem can be partially solved by adding a small positive constant to the IRF denominator, without significantly increasing the much greater low-frequency components that are more relevant for deconvolution [39]. Addition of this constant is equivalent to adding a delta peak at the start of the IRF, as illustrated in figure 2 (right). The spectral offset at high frequencies can be seen in figure 3 (left).

3. Filtering: the resulting deconvoluted signal was filtered with a low pass first order Butterworth

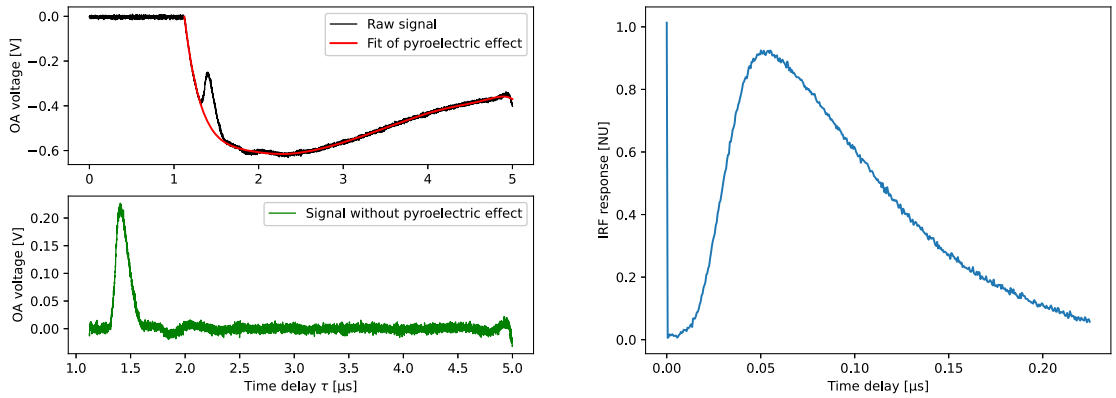

Figure 2. Left: process of removal of the pyroelectric effect. Top: raw signal from OA (black), fit of the pyroelectric effect with polynomial (red). Bottom: the OA signal after the pyroelectric effect is removed. Right: the impulse response function (IRF) of the OA detector, measured with the a single pulse on a thin black tape. The single delta peak at the beginning is added in order to create an offset to the IRF spectra.

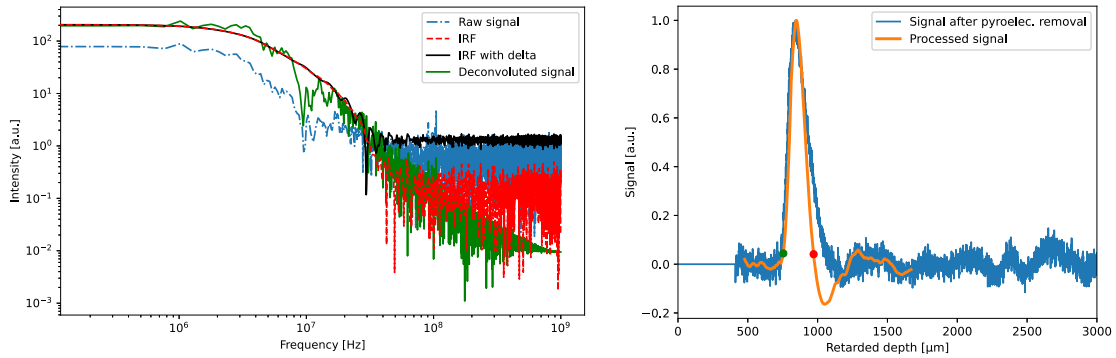

Figure 3. Left: Fourier transformations of the initial raw signal, IRF, IRF with added delta peak and resulting deconvoluted signal. Note the spectral offset of the IRF at high frequencies after adding the delta peak at its beginning. Right: the processed OA signal after removing of the pyroelectric effect (blue), low-pass filtering and deconvolution. The green and red dots mark the start and the end points of the OA compression phase that corresponds to the thickness of the skin lesion.

filter, with empirically found cutoff frequency of 20 MHz. This reduces the remaining ringing noise and parasitic signals that dominate after deconvolution [40].

The resulted signal shows the measured stress profile that is related to the depth absorption profile of the lesion. Due to the large size of the excitation area and the small distance between the PDVF detector and the sample inside the PMMA layer, the OA signal can be considered within the acoustical near-field approximation [33, 34]. Within this model, the thickness of the first absorbing layer is simply the width of the compression peak. This compression phase is followed by a sharp rarefaction dip, caused by the sudden decrease of the absorption coefficient of the nevus. The width was measured automatically by finding the rising and the falling points of the compression phase, as shown in figure 3 (right). The starting compression point is found by taking the position of maximum of the second derivative of the OA signal. The end point was chosen as the time point when the signal reached the level of the previously found start point. The measured thickness is then the difference between these points. This resulting width was defined as the OA thickness. We estimate that it is correlated with the thickness of the lesion underneath the detector due to the increased absorption of radiation at a wavelength of 532 nm. The proposed signal processing technique has been previously tested on layered polyvinyl alcohol based hydrogel (PVA-H) tissue phantoms, which also showed good correlation with numerical simulations in near-field acoustical propagation [36, 37].

7 different patients in the age range between 20 and 60 years, 4 females and 3 males, all of Caucassian skin type were recruited, with a total of 9 suspicious skin lesions. The performed measurements were approved by the Ethics Committee of the University Medical Center Rostock (A 2016-0115) and met the principals of the Declaration of Helsinki. Each participant gave his written consent for participation in the presented study.

Each measurement was performed 10 times on each lesion, at roughly the center spot of the nevus and immediately afterwards the lesions were excised for histological measurements. The maximal lesion thickness was

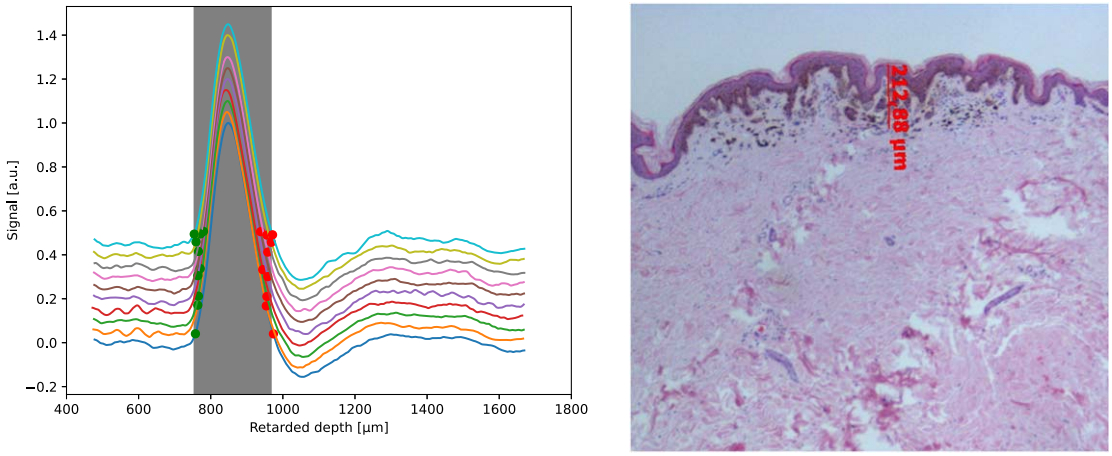

Figure 4. Left: an example of 10 consequent processed OA signals of a single lesion. The red and green circles mark the beginning and the end of the compression phase, thus pointing to the measurable lesion depth. The grey shaded area represents the measured histological thickness of 191 μm. Right: the corresponding histological measurement which was determined close to the OA result. Red annotation represents the maximal lesion depth of 213 μm found by the dermatologist.

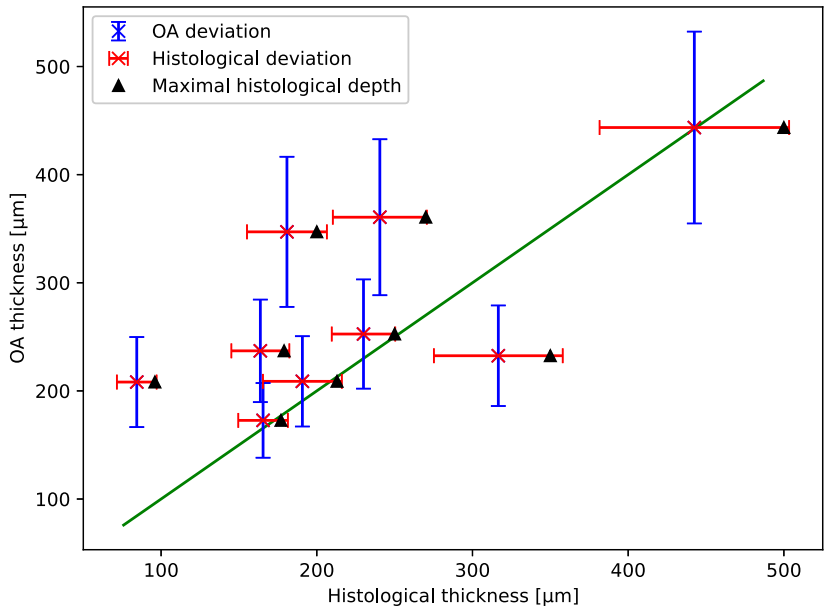

Figure 5. Comparison of the OA thickness results (y-axis) and the corresponding histological thickness measurements from 9 suspicious skin lesions (x-axis). The black triangles represent the maximal histological depth measured by the dermatologist; the red crosses show the mean depth around that point within a range of ± 1 mm. The green line represents the 1:1 agreement line.

identified and measured by a dermatologist. Around this position the lesion thickness was measured at multiple locations within ± 1 mm range, since it is considered to be the integration zone of the OA detector.

3. Results and discussion

Similar to the measurements on PVA-H phantoms, the OA signal on lesions shows similar compression and rarefaction phases and the OA thickness is found to be correlated to the histological depth. An exemplary measurement of a single lesion with 10 consequent pulses is shown in figure 4 (left), together with the corresponding histological measurement (right). The OA thickness yielded 209 μm, which correlates well with the mean histological depth of 191 μm and maximal lesion depth of 213 μm.

The OA depth measurements and the comparison to the immediate histological results are presented in figure 5. The thicknesses of 9 lesions ranged between 100 μm and 450 μm are presented in this work. Several measurements that deviate from the histology were problematic due to the uneven or rough surface of the lesion, which resulted in several reflected compression phases due to the bad acoustical coupling with the detector and therefore apparent larger width. Overall, the OA results show qualitative correlation with the histological measurements, with largest deviations for

the lesions with 100 μm and 350 μm. Except the latter measurement, the OA tends to overestimate the thickness compared to histology. Interestingly, Varketin *et al* [41] also report overestimation of OCT and HFUS thickness measurements for lesions with histological thickness $<$0.2 mm, and strong underestimation of thicknesses $>$0.5 mm. Similarly, photoacoustic microscopy (PAM) results of Breathnach *et al* [42] *in vivo* and the results of Zhou *et al* [25, 43] also indicate overestimation of OA thickness results with histological depths.

One possible reason for overestimation is the shrinking of tissue, since it is known that the excision and the following fixation, dehydration and paraffinization of the tissue lead to tissue deformations [44]. Additional deviation can be also explained by uneven or rough surface of the lesion, which resulted in several reflected compression phases due to the non-ideal acoustical coupling with the detector and therefore apparent larger width. Finally, it cannot be precisely ensured that the excision will be sliced and histologically imaged at the same position where the OA measurement was taken; the solution to this problem requires OA measurements at multiple positions, which is planned in the future work.

All in all, the results indicate correlation between the lesion depths for lesion infiltration depths below 500 μm. This simple technique can thus allow the dermatologist to estimate the depth of the lesion and as a result its condition, and assist the surgeon to choose the correct excision depth. In the future work it is intended to implement a translation to the OA detector, thus allowing to establish a 3D depth profile map of the nevi and measure their size more accurately. However, in this case, the correlation with the histological thickness determination has to be worked out, as the latter is confined to one plane through the nevus. For strongly pigmented skin lesions with thickness less than 200 μm, OCT can be utilized to establish the 3D depth profile of the nevus and validate the OA measurements [45, 46]. In order to achieve larger penetration depth for the OA modality, longer OA excitation wavelengths generated by an optical parametric oscillator will be used in the next step. In future work, the developed OA detector will be integrated with a translational system and other optical modalities, such as Raman spectroscopy and optical coherence tomography, that will provide additional information on chemical and morphological structure of skin lesions and aid in the diagnosis. The integration with Raman spectroscopy is of a particular benefit, as the laser pulses can be used for simultaneous measurement of Raman and OA and therefore no additional optical excitation will be required. The transparency of the detector in the visible range allows to place it directly in the optical path of other modalities and thus achieve spatial localization of measurements. In addition, it is planned to investigate different launching angles for excitation pulses, as they play a significant role in generation of OA signals [35].

4. Conclusion

In this work we have presented the first results of depth measurements of suspicious skin lesions *in vivo* on humans with a transparent OA detector while staying at a third of the MPE limits. After the signal processing and deconvolution with the previously measured IRF function, the OA signals reveal compression peaks whose width show correlation with the immediate histological results, as expected from the acoustical near-field theory with flat nevi. On average, the OA slightly overestimates the mean histological lesion depth, possibly due to the axial tissue shrinkage during the fixation process and it is similar to other pilot studies. We believe that this simple method can assist the dermatologist to measure lesion depths non-invasively and estimate the safety excision margins and thus, shorten the time to diagnosis. As the required exposure is at a third of the MPE levels, it allows for further exposure with lateral scanning or other optical modalities.

Acknowledgments

The authors acknowledge financial support from the German Research Foundation DFG (German Research Foundation, Project ID RO 3471/18-1 and EM 63/13-1). We thank Prof. Steffen Emmert from the University Hospital of Rostock for allowing to perform the OA measurements on volunteered patients and providing us with histological results. Also, financial support by the Deutsche Forschungsgemeinschaft (DFG, German Research Foundation) under Germany's Excellence Strategy within the Cluster of Excellence PhoenixD (EXC 2122, Project ID 390833453) is acknowledged.

Data availability statement

The data that support the findings of this study are available upon reasonable request from the authors.

ORCID iDs

Anatoly Fedorov Kukk https://orcid.org/0000-0003-2233-4960
Bernhard Roth https://orcid.org/0000-0001-9389-7125

References

[1] Bhatia S, Tykodi S S and Thompson J A 2009 Treatment of metastatic melanoma: an overview *Oncology (Williston Park, NY)* **23** 488–96
[2] Wang T, Qiu J and Milner T E 2011 Determination of melanoma lateral and depth margins: potential for treatment planning and five-year survival rate *Skin Cancer Overview* 1 (London, United Kingdom: IntechOpen) p 109–40 (http://intechopen.com/books/skin-cancer-overview/determination-of-melanoma-lateral-and-depth-margins-potential-for-treatment-planning-and-five-year-s)

[3] Szeimies R M, Hauschild A, Garbe C, Kaufmann R and Landthaler M 2010 *Tumoren der Haut: Grundlagen, Diagnostik und Therapie in der dermatologischen Onkologie* (Stuttgart, Germany: Thieme Medical Publishers/Georg Thieme Verlag) (https://doi.org/10.1055/b-002-37780)
[4] Meyer N, Lauwers-Cances V, Lourari S, Laurent J, Konstantinou M-P, Lagarde J-M, Krief B, Batatia H, Lamant L and Paul C 2014 High-frequency ultrasonography but not 930-nm optical coherence tomography reliably evaluates melanoma thickness *in vivo*: a prospective validation study *British Journal of Dermatology* **171** 799–805
[5] Bozsányi S *et al* 2022 Multispectral imaging algorithm predicts breslow thickness of melanoma *Journal of Clinical Medicine* **11** 189
[6] Yew E, Rowlands C and So P T C 2014 Application of multiphoton microscopy in dermatological studies: a mini-review *Journal of Innovative Optical Health Sciences* **7** 1330010
[7] Que S K T 2016 Research techniques made simple: noninvasive imaging technologies for the delineation of basal cell carcinomas *Journal of Investigative Dermatology* **136** e33–8
[8] Elagin V, Gubarkova E, Garanina O, Davydova D, Orlinskaya N, Matveev L, Klemenova I, Shlivko I, Shirmanova M and Zagaynova E 2021 In vivo multimodal optical imaging of dermoscopic equivocal melanocytic skin lesions *Scientific Reports* **11** p1–12
[9] Manohar S and Razansky D 2016 Photoacoustics: a historical review *Advances in Optics and Photonics* **8** 586–617
[10] Maslov K, Hu S and Wang L V 2011 Second generation optical-resolution photoacoustic microscopy *Proc. SPIE* **7899** 789933 (https://spiedigitallibrary.org/conference-proceedings-of-spie/7899/789933/Second-generation-optical-resolution-photoacoustic-microscopy/10.1117/12.874786.short?SSO=1)
[11] Yao J, Maslov K I, Zhang Y, Xia Y and Wang L V 2011 Label-free oxygen-metabolic photoacoustic microscopy *in vivo* *J. Biomed. Opt.* **16** 1076003
[12] Park B, Bang C H, Lee C, Han J H, Choi W, Kim J, Park G S, Rhie J W, Lee J H and Kim C 2021 3D wide-field multispectral photoacoustic imaging of human melanomas *in vivo*: a pilot study *Journal of the European Academy of Dermatology and Venereology* **35** 669–76
[13] Qi W, Jin T, Rong J, Jiang H and Xi L 2017 Inverted multiscale optical resolution photoacoustic microscopy *J. Biophotonics* **10** 1580–5
[14] Li M *et al* 2018 Linear array-based real-time photoacoustic imaging system with a compact coaxial excitation handheld probe for noninvasive sentinel lymph node mapping *Biomedical Optics Express* **9** 1408–22
[15] Dahlstrand U, Sheikh R, Merdasa A, Chakari R, Persson B, Cinthio M, Erlöv T, Gesslein B and Malmsjö M 2020 Photoacoustic imaging for three-dimensional visualization and delineation of basal cell carcinoma in patients *Photoacoustics* **18** 100187
[16] Wang L V 2009 Multiscale photoacoustic microscopy and computed tomography *Nat. Photonics* **3** 503–9
[17] Zhang W, Li Y, Nguyen V P, Huang Z, Liu Z, Wang X and Paulus Y M 2018 High-resolution, *in vivo* multimodal photoacoustic microscopy, optical coherence tomography, and fluorescence microscopy imaging of rabbit retinal neovascularization *Light: Science & Applications* **7** 1–12
[18] Wang L V and Yao J 2016 A practical guide to photoacoustic tomography in the life sciences *Nat. Methods* **13** 627–38
[19] Wang L V and Hu S 2012 Photoacoustic tomography: *in vivo* imaging from organelles to organs *Science* **335** 1458–62
[20] Xia J, Yao J and Wang L V 2014 Photoacoustic tomography: principles and advances *Electromagnetic Waves (Cambridge, Mass.)* **147** 1
[21] Zhou Y, Wang D, Zhang Y, Chitgupi U, Geng J, Wang Y, Zhang Y, Cook T R, Xia J and Lovell J F 2016 A phosphorus phthalocyanine formulation with intense absorbance at 1000 nm for deep optical imaging *Theranostics* **6** 688
[22] Hu S, Maslov K and Wang L V 2011 Second generation optical-resolution photoacoustic microscopy with improved sensitivity and speed *Optics letters* **36** 1134–6 (http://opg.optica.org/ol/abstract.cfm?URI=ol-36-7-1134)
[23] Jo J, Xu G, Marquardt A, Girish G and Wang X 2017 Photoacoustic evaluation of human inflammatory arthritis in human joints *Proc. SPIE* **10064** 1006409P
[24] Park J, Park B, Kim T, Lee D, Yong U, Jang J, Jeong U, Kim H H and Kim C 2020 Seamlessly integrated optical and acoustical imaging systems through transparent ultrasonic transducer *Photons Plus Ultrasound: Imaging and Sensing 2020* vol 11 240 *(San Francisco, California, United States, 17 February 2020)* ed A A Oraevsky and L V Wang (International Society for Optics and Photonics) 112401
[25] Zhou Y, Li G, Zhu L, Li C, Cornelius L A and Wang L V 2015 Handheld photoacoustic probe to detect both melanoma depth and volume at high speed *in vivo J. Biophotonics* **8** 961–7
[26] Leng H *et al* 2019 Characterization of a fiber bundle-based real-time ultrasound/photoacoustic imaging system and its *in vivo* functional imaging applications *Micromachines* **10** 820
[27] Niederhauser J J, Jaeger M, Hejazi M, Keppner H and Frenz M 2005 Transparent ito coated pvdf transducer for optoacoustic depth profiling *Opt. Commun.* **253** 401–6
[28] Park J *et al* 2021 Quadruple ultrasound, photoacoustic, optical coherence, and fluorescence fusion imaging with a transparent ultrasound transducer *Proc. Natl Acad. Sci.* **118** e1920879118
[29] 2018 Bundesanstalt für Arbeitsschutz und Arbeitsmedizin. Teil 2: Messungen und berechnungen von expositionen gegenüber laserstrahlung. Technische Regeln zur Arbeitsschutz-verordnung zu künstlicher optischer Strahlung. (https://baua.de/DE/Angebote/Rechtstexte-und-Technische-Regeln/Regelwerk/TROS/TROS-Laser-Teil-2.html)
[30] 2007 ANSI Z136.1 - American National Standard for Safe Use of Lasers
[31] Ren D, Sun Y, Shi J and Chen R 2021 A review of transparent sensors for photoacoustic imaging applications *Photonics* **vol 8** p 324
[32] Möller E 2020 *Handheld optoacoustic probe facilitating nearfield investigations through a transparent detector* Doctoral dissertation, Hannover: Gottfried Wilhelm Leibniz Universität (https://repo.uni-hannover.de/handle/123456789/10270)
[33] Stritzel J, Melchert O, Wollweber M and Roth B 2017 Effective one-dimensional approach to the source reconstruction problem of three-dimensional inverse optoacoustics *Phys. Rev. E* **96** 033308
[34] Melchert O, Wollweber M and Roth B 2019 Optoacoustic inversion via convolution kernel reconstruction in the paraxial approximation and beyond *Photoacoustics* **13** 1–5
[35] Sivasubramanian K, Periyasamy V, Wen K K and Pramanik M 2016 Optimizing light delivery through fiber bundle in photoacoustic imaging with clinical ultrasound system: Monte carlo simulation and experimental validation *J. Biomed. Opt.* **22** 041008
[36] Blumenröther E, Melchert O, Wollweber M and Roth B 2016 Detection, numerical simulation and approximate inversion of optoacoustic signals generated in multi-layered pva hydrogel based tissue phantoms *Photoacoustics* **4** 125–32
[37] Melchert O, Blumenröther E, Wollweber M and Roth B 2018 Numerical prediction and measurement of optoacoustic signals generated in PVA-H tissue phantoms *European Physical Journal D* **72** 1–11
[38] Moran C M, Bush N L and Bamber J C 1995 Ultrasonic propagation properties of excised human skin *Ultrasound Med. Biol.* **21** 1177–90
[39] O'Haver T 1997 *A pragmatic introduction to signal processing.* (University of Maryland at College Park: Independently published)
[40] Blumenröther E, Melchert O, Kanngießer J, Wollweber M and Roth B 2019 Single Transparent Piezoelectric Detector for Optoacoustic Sensing-Design and Signal Processing *Sensors* **19** 1–11
[41] Varkentin A, Mazurenka M, Blumenröther E, Meinhardt-Wollweber M, Rahlves M, Broekaert S M C,

Schäd-Trcka S, Emmert S, Morgner U and Roth B 2017 Comparative study of presurgical skin infiltration depth measurements of melanocytic lesions with oct and high frequency ultrasound *J. Biophotonics* **10** 854–61

[42] Breathnach A, Concannon E, Dorairaj J J, Shaharan S, McGrath J, Jose J, Kelly J L and Leahy M J 2018 Preoperative measurement of cutaneous melanoma and nevi thickness with photoacoustic imaging *Journal of Medical Imaging* **5** 015004

[43] Zhou Y, Xing W, Maslov K I, Cornelius L A and Wang L V 2014 Handheld photoacoustic microscopy to detect melanoma depth *in vivo Opt. Lett.* **39** (16) 4731-4734

[44] Plekhanov A A, Sirotkina M A, Sovetsky A A, Gubarkova E V, Kuznetsov S S, Matveyev A L, Matveev L A, Zagaynova E V, Gladkova N D and Zaitsev V Y 2020 Histological validation of *in vivo* assessment of cancer tissue inhomogeneity and automated morphological segmentation enabled by optical coherence elastography *Sci. Rep.* **10** 1–16

[45] Rahlves M, Varkentin A, Stritzel J, Blumenroether E, Mazurenka M, Wollweber M and Roth B 2016 Towards multimodal detection of melanoma thickness based on optical coherence tomography and optoacoustics *Proc. SPIE* **9701** 97010F

[46] Varkentin A, Mazurenka M, Blumenröther E, Behrendt L, Emmert S, Morgner U, Meinhardt-Wollweber M, Rahlves M and Roth B 2018 Trimodal system for *in vivo* skin cancer screening with combined optical coherence tomography-raman and colocalized optoacoustic measurements *J. Biophotonics* **11** e201700288